Journal of
Materials Chemistry A

RSC Publishing

PAPER

View Article Online
View Journal | View Issue

Cite this: *J. Mater. Chem. A*, 2013, **1**, 9477

Magnetic hollow carbon nanospheres for removal of chromium ions

Lu-Hua Zhang, Qiang Sun, Dong-Hai Liu and An-Hui Lu*

Received 29th January 2013
Accepted 22nd March 2013

DOI: 10.1039/c3ta10430c

www.rsc.org/MaterialsA

Magnetically functionalized carbon materials as adsorbents have shown outstanding adsorption capacity for Cr(VI) removal. Here, magnetic hollow carbon nanospheres (MHCSs) have been fabricated by simply changing the pyrolysis temperature from 600 to 850 °C of the polymer counterparts, which were denoted as MHCS-*n*, where *n* is 600, 700, or 850 °C. The MHCS composite displayed spherical morphology with a hollow air core and crack-free carbon shell structure, which was homogenously and controllably loaded with nanosized (*ca.* 10 nm) Fe-based nanoparticles (*ca.* 8.9 wt%). In principle, the hollow structure would allow more exposed adsorption sites to adsorbate than a solid structure. When evaluated as an absorbent for Cr(VI) ion removal, such highly engineered MHCSs exhibited excellent adsorption capacity. The maximum adsorption capacity of Cr(VI) per weight of adsorbent was 200 mg g^{-1}, which was much higher than those of other carbon-based adsorbents reported in literature. The extraordinary adsorption capacity of MHCS-700 may be attributed to two factors: (i) the large specific surface area would provide abundant functional groups, (ii) the developed graphitic structures provide electrostatic interactions between π electrons and Cr species. Furthermore, magnetic iron-based nanoparticles allowed fast separation of the MHCSs from liquid suspension. Thus, the MHCSs may serve as an ideal candidate for chromium removal in water treatment.

1 Introduction

With the population explosion, agricultural activities, industrialization and other geological and environmental changes, the quality of our water resources is unfortunately deteriorating continuously. Thousands of organic, inorganic, and biological pollutants have been reported as water contaminants. Heavy metals, such as chromium, cadmium, arsenic, cobalt, copper, selenium, miscellaneous metal ions, *etc.*, are known as some of the most familiar inorganic contaminants for their high toxicity, carcinogenicity and bioaccumulation in the human body through the food chain.[1] Of these, the pollution of Cr(VI) exists widely because they are prevailingly used in and generated by a large amount of industrial processes, including leather tanning, electroplating, metal polishing, dye and pigment manufacture.[2,3] Besides, Cr(VI) ions are highly soluble and mobile in aquatic systems, causing extremely negative impacts on plants, animals and human health.[4]

Various approaches have been developed for the removal of Cr(VI).[5,6] Among them, adsorption technology is more and more investigated in fundamental studies and industrial applications because of its ease and safety of operation, versatility for different water streams,[7] and the availability of a wide range of adsorbents. In recent years, a number of carbonaceous adsorbents, namely activated carbons (ACs)[8] and oxidized AC,[9] have been prepared and used for the removal of Cr(VI) ions owing to their low cost, acid and alkali corrosion resistance, high specific surface area and enhanced adsorption capacity for the heavy metal. However, there is a big issue in the utilization of these materials, for the reason that conventional separation methods, including filtration and centrifugation, are time consuming and likely to lose adsorbents. Therefore, it is very intriguing to develop innovative adsorbents which can be easily and quickly removed from aqueous systems. Magnetically functionalized carbon materials have entered into our sight because of the impact for improving adsorption capacity and easy separation under an external magnetic field.[10–17] Despite the fact that a variety of magnetic carbon-based adsorbents, as the most promising ones given their high maximum adsorption capacity (Q_m) of removing chromium, have been reported, such as magnetic graphene (0.95 mg g^{-1}),[10] γ-Fe_2O_3/CMK-3 (30 mg g^{-1}),[14] MWCNTs/Fe_2O_3 (90 mg g^{-1}),[15] chitosan modified Fe^0 nanowires embedded in PAA (113.2 mg g^{-1})[16] and magnetic β-cyclodextrin/graphene oxide nanocomposite (120.19 mg g^{-1}),[17] it is still an ongoing challenge to create highly efficient Cr(VI) adsorbents that present easy separation and large adsorption capacity.

Herein, we report the fabrication of magnetic hollow carbon nanospheres *via* simply pyrolyzing the polymer counterparts,

State Key Laboratory of Fine Chemicals, School of Chemical Engineering, Faculty of Chemical, Environmental and Biological Science and Technology, Dalian University of Technology, Dalian 116024, P.R. China. E-mail: anhuilu@dlut.edu.cn; Fax: +86-411-84986112; Tel: +86-411-84986112

which are prepared based on the weak acid–base interaction induced assembly.[18] The MHCS composites displayed spherical morphology with a hollow air core and crack-free carbon shell structure anchored with magnetic iron-based nanoparticles. To our knowledge, nanosized hollow structures with large size cavity possess intrinsic advantages of high external surface area compared to their solid counterparts on the basis of unit mass, and allow full utilization of the active sites.[19,20] Additionally, iron-based nanoparticles can be magnetically separated when external magnetic fields are introduced.[21,22] One thus can envisage that the adsorbents with the advantages mentioned above would show superior adsorption capacity. Importantly, when used as the adsorbents in Cr(VI) removal, MHCSs indeed exhibit superior adsorption capacity and easy magnetic separation. The maximum adsorption capacity of Cr(VI) per weight of adsorbent is 200 mg g^{-1}, which is much higher than those of other carbon-based adsorbents reported so far in literature.[8–10,14–17]

2 Experimental

2.1 Chemicals

2,4-Dihydroxybenzoic acid (DA) was obtained from Aldrich. Sodium oleate, formaldehyde, $FeCl_3 \cdot 6H_2O$, and potassium dichromate were obtained from the Sinopharm Chemical Reagent Co. All chemicals were used as received without any further purification.

2.2 Synthesis of hollow polymer nanospheres

Based on the previous synthesis[18] but with a slight modification, herein, we chose sodium oleate as the surfactant in order to obtain hollow polymer nanospheres (HPSs) with large size cavity which might be beneficial for Cr(VI) adsorption. Firstly, 2.5 mmol of 2,4-dihydroxybenzoic acid, 7.5 mmol of formaldehyde and 180 μL of ammonia solution (25%) were dissolved in 95 mL of deionized water. A 5 mL volume of an aqueous solution containing 0.18 mmol of sodium oleate was added to the above-prepared solution at 30 °C under slow stirring (100 rpm). The mixture solution was stirred for 30 min to yield a stable emulsion and then transferred into an autoclave hydrothermally aged for 4 h at the temperature of 120 °C. The resulting HPSs were retrieved by centrifugation (8000–9000 rpm, 10 min), then washed with deionized water and ethanol.

2.3 Synthesis of magnetic hollow carbon nanospheres

First, HPSs were immersed in aqueous $FeCl_3 \cdot 6H_2O$ (0.24 M) for 12 h to load Fe^{3+} to obtain HPS–Fe, and subsequently washed with deionized water and ethanol, then dried at 50 °C for 6 h. Subsequently, the obtained polymeric spheres HPSs–Fe were pyrolyzed at the desired temperature (*e.g.* 600, 700, or 850 °C), with a heating rate of 3 °C min^{-1} and kept at that temperature for 4 h under nitrogen atmosphere. Finally, magnetic hollow carbon nanospheres were synthesized, which were accordingly named as MHCS-600, MHCS-700, MHCS-850.

2.4 Cr(VI) removal experiments

Typically, 20 mg of the sample was added to 100 mL solution of $K_2Cr_2O_7$ in distilled water (different concentrations of Cr(VI): 5, 10, 15 mg L^{-1}) and stirred at room temperature for 24 h in a closed vessel. The pH of the suspensions was adjusted to 3 by adding HCl solution (0.1 M). During the adsorption process, at different periods (0, 0.5, 2, 4, 6, 9, 12, and 24 h), about 0.3 mL of the Cr(VI) solution was extracted with a needle tube equipped with a membrane filter and then diluted to be used for colorimetric measurements. The obtained solutions were determined using the 1,5-diphenylcarbazide method.[23] In particular, 3 mL of the ultimate Cr(VI) solution at different periods was mixed with 120 μL 1,5-diphenylcarbazide solution (0.025 g 1,5-diphenylcarbazide in 10 mL of acetone) and 60 μL H_3PO_4 solution (0.5 mL H_3PO_4 (85%) in 10 mL of H_2O). The solution was left for 10 min to allow color development, and then the solution's concentration was determined by UV-vis spectrophotometry at 540 nm.

2.5 Characterization

The X-ray diffraction (XRD) measurements were recorded with a Rigaku D/Max 2400 diffractometer using Cu Kα radiation (λ = 0.15406 nm). Transmission electron microscopy (TEM) analyses were carried out with Tecnai $G^2$20S-Twin equipment operating at 200 kV. The IR spectra were collected on a Nicolet 6700 Fourier transform infrared (FTIR) spectrometer. Nitrogen adsorption isotherms were measured with an ASAP 2020 adsorption analyzer at 77 K. The Brunauer–Emmett–Teller (BET) method was utilized to calculate the specific surface areas. The total pore volumes were estimated from the amount adsorbed at a relative pressure of 0.90. The micropore volumes were calculated using the *t*-plot method. The thermal decomposition behavior of the products was monitored using a simultaneous thermal analyzer (Netzsch STA 449 F3), with a heating rate of 10 °C min^{-1}.

3 Results and discussion

3.1 Structure properties of the MHCSs

In our previous work,[18] hollow polymer nanospheres (HPSs) exhibiting controllable sizes and a functionalizable shell were prepared through the weak acid–base ($COO^-/NH_4^+/COO^-$) interaction induced assembly under hydrothermal conditions. In this paper, in order to prepare HPSs with larger size cavity, sodium oleate was selected to serve as the surfactant to create the suitable emulsion. After mixing the sodium oleate solution and DA/formaldehyde solution, the emulsion was formed immediately. Ammonium ions could bridge the emulsion droplets and DA by weak acid–base interactions[24] and guided the assembly of DA and formaldehyde around the emulsion in the following polymerization process to form the functional shells. SEM and TEM images of the HPSs show spherical morphology with a well-defined core–shell structure, with an average diameter of 200 nm and core diameter of 100 nm (Fig. 1a and b). Compared with the oleic acid/ammonia/DA/formaldehyde system reported previously,[18] the HPSs here

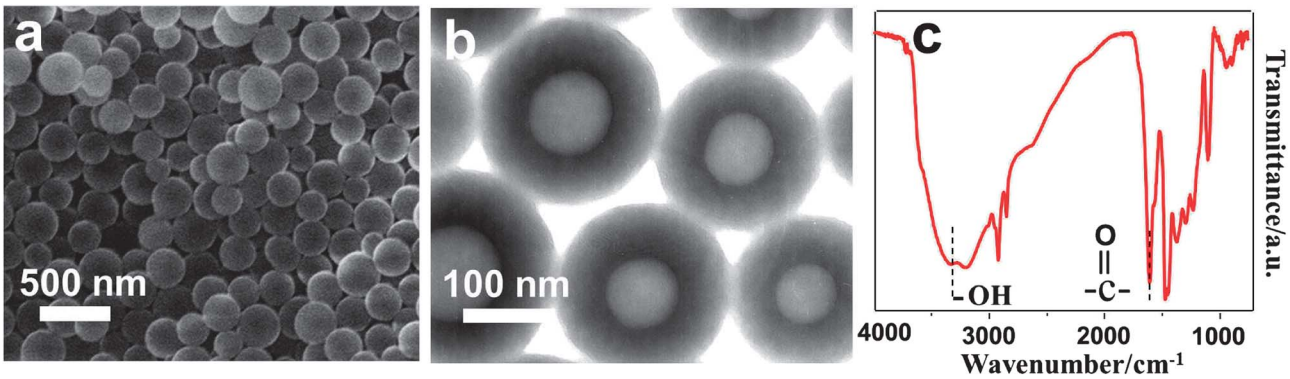

Fig. 1 SEM image (a), TEM image (b), and FT-IR spectrum (c) of HPSs.

possessed larger hollow interiors. This phenomenon might be attributed to the difference in the emulsion formation process. The surface functional groups of the HPSs were examined by FT-IR spectroscopy (Fig. 1c). The broad absorption peaks at 3400 cm^{-1} and 1750 cm^{-1} observed are assigned to the vibrating peaks of the hydroxyl (–OH) and carboxyl groups (–C=O–), respectively. Owing to the abundant carboxyl groups, Fe^{3+} ions could be introduced into HPSs through an ion-exchange process.[26,27] The final product MHCSs can be obtained by simply changing the pyrolysis temperature of hollow polymeric spheres containing Fe^{3+} ions (HPSs–Fe) from 600 to 850 °C .

As we all know, the pyrolysis temperature is a main factor influencing the structure and composition of a carbon product. Consequently, the pyrolysis of HPSs–Fe was conducted at different desired temperatures (*e.g.* 600, 700, or 850 °C). With an increase in pyrolysis temperature, the carbon residues (experimental data) for MHCS-600, MHCS-700 and MHCS-850 are 46 wt%, 41 wt% and 38 wt%, respectively. The development of the specific surface areas and total pore volumes was detected using the liquid nitrogen adsorption technique. The N_2 adsorption isotherms of all MHCS samples are shown in Fig. 2a. The specific surface areas (S_{BET}) and total pore volumes (V_{total}) of the samples decreased with increasing pyrolysis temperature (Table 1). The S_{BET} of MHCS-600, MHCS-700 samples are 490, 453 $m^2\ g^{-1}$ and V_{total} are 0.26, 0.28 $cm^3\ g^{-1}$, respectively. As the pyrolysis temperature increased to 850 °C, the surface area sharply decreased to 217 $m^2\ g^{-1}$, meanwhile the total pore volume decreased to 0.15 $cm^3\ g^{-1}$. The reason for the sharp decreases of S_{BET} and V_{total} was that higher pyrolysis temperature resulted in higher graphitization degree of carbons, and formation of graphitic carbon by sacrificing the microporosity and low density.[28,29] The iron contents of MHCSs were evaluated by thermogravimetric analysis. At the end, the iron compounds are expected as Fe_2O_3 after combustion in air. TG result in Fig. 2c demonstrate that the contents of Fe_2O_3 are accordingly 10.3 wt% for MHCS-600, 11.7 wt% for MHCS-700 and 12.7 wt% for MHCS-850. Thus the Fe contents are calculated to be 7.2 wt %, 8.2 wt% and 8.9 wt% (Table 1). Magnetic properties were studied using a vibrating sample magnetometer. Magnetization curves in Fig. 2d show that MHCSs exhibit ferromagnetic behavior. Their saturation magnetization values are in the range of 2.9–4.3 emu g^{-1}, indicating a magnetic separation capability.[30]

To establish the crystal phases of the iron-based nanoparticles, the obtained MHCS samples were characterized by XRD. As shown in Fig. 3a, the diffraction peaks of MHCS-600 are well in accordance with the standard diffraction pattern of Fe_3O_4 (magnetite, JCPDS, no. 85-1436). Along with the temperature increase, the diffraction peak at 26.5° can be assigned to the (002) planes of graphitic carbon, which is further confirmed by the Raman spectrum (Fig. 2c). The new diffraction peaks at 44.8° and 65.1° indicate the presence of α-Fe (JCPDS no. 06-0696). The rest of the diffraction peaks correspond to the crystal planes of Fe_3C species (JCPDS, no. 89-2867). To further determine the types of iron compounds, we measured the ^{57}Fe Mössbauer spectra of MHCS-700 at room temperature (Fig. 3b). As the pyrolysis temperatures increased to 700 °C, Fe_3O_4 was almost completely converted to Fe and Fe_3C (Table 2). Mössbauer analysis is in good agreement with the XRD result.

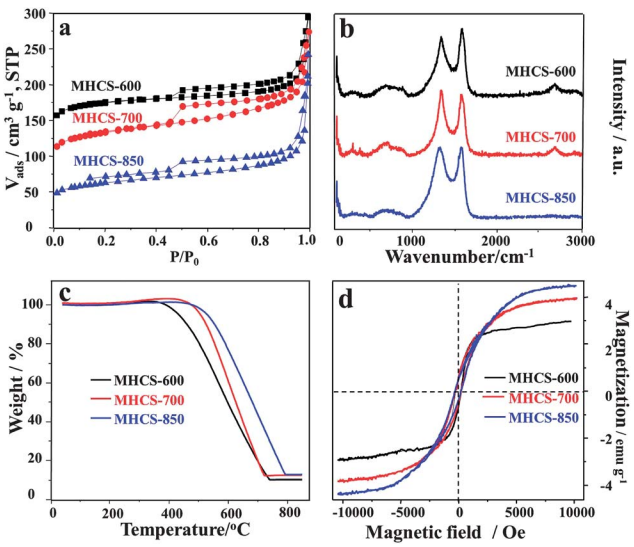

Fig. 2 N_2 sorption isotherms (a), Raman spectra (b), TGA curves in air (c), and room temperature magnetization curves (d) of MHCS-600, MHCS-700 and MHCS-850. Note that the N_2 sorption isotherm of MHCS-600 is offset vertically by 30 $cm^3\ g^{-1}$ STP.

Table 1 Structural and textural parameters of the magnetic hollow carbon nanospheres

Sample	S_{BET}[a] ($m^2\ g^{-1}$)	V_{mic}[b] ($cm^3\ g^{-1}$)	V_{total}[c] ($cm^3\ g^{-1}$)	Iron (wt%)	Fe_2O_3 (wt%)	M_s[d]
MHCS-600	490	0.18	0.26	7.2	10.3	2.9
MHCS-700	453	0.14	0.28	8.2	11.7	4.0
MHCS-850	217	0.05	0.15	8.9	12.7	4.3

[a] S_{BET}: specific surface area calculated by the BET method at a P/P_0 range of 0.05–0.3. [b] V_{mic}: micropore volume calculated by the *t*-plot method. [c] V_{total}: total pore volume at $P/P_0 = 0.90$. [d] M_s: magnetic saturation value.

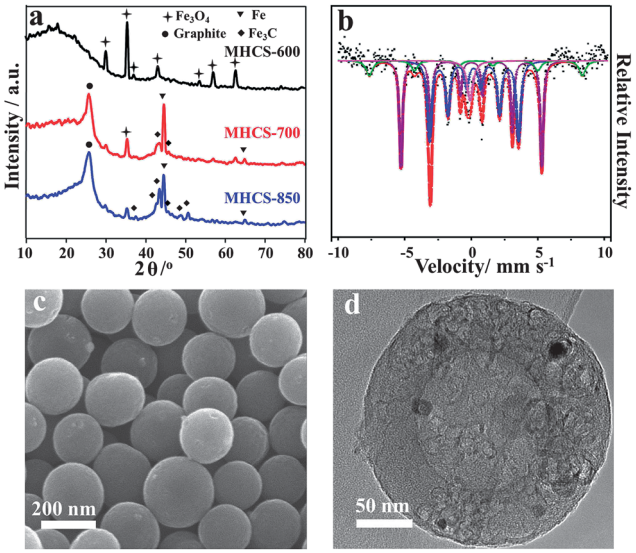

Fig. 3 XRD patterns of MHCS-600, MHCS-700 and MHCS-850 (a); room temperature measured ^{57}Fe Mössbauer spectra (b), SEM image (c) and TEM image (d) of MHCS-700.

The textural properties of obtained MHCS-700 were characterized by SEM and TEM. As shown in Fig. 3c and d, the hollow core–shell nanostructures are retained after pyrolysis, and the sphere size and shell thickness of MHCS-700 are about 200 and 50 nm, respectively. The TEM image in Fig. 3d shows that the hollow carbon spheres consist of well-developed nanosized turbostratic graphite structures, and the growth of graphitic carbons appeared strictly confined within the shell. This pseudomorphic transformation phenomenon has previously been observed by us.[25,26] The dark spots in Fig. 3c and d indicate the *in situ* formed Fe/Fe_3C nanoparticles. The graphitized nature and crystallization of iron species in the MHCSs were also in agreement with XRD (Fig. 3a) and Raman analyses (Fig. 2b).

3.2 Remediation experiments for Cr(VI) removal from aqueous solutions

The adsorption capacities and kinetics of the MHCSs for removing Cr(VI) from acid aqueous solutions (pH = 3) were investigated by conducting a series of kinetic experiments. Fig. 4 shows the performance of MHCS-600, MHCS-700 and MHCS-850 in Cr(VI) removal under the conditions of initial solution concentrations (5, 10 and 15 mg L^{-1}), the solution volume of 100 mL, and adsorption temperature of 25 °C. In the case of the starting solution with a concentration of 5 mg L^{-1}, all the samples show a final removal efficiency of 100% (Fig. 4a). Further increasing the concentration to 10 mg L^{-1}, samples MHCS-600 and MHCS-700 exhibit higher effectiveness in Cr(VI) removal than sample MHCS-850 (Fig. 4b). This was attributed to the large specific surface areas of MHCS-600 and MHCS-700 that provide abundant functional groups and can interact with Cr(VI). Similarly, even though the concentration of Cr(VI) in the influent is 15 mg L^{-1}, the adsorption capacity of sample MHCS-700 can still reach 100% of the total chromium amount (Fig. 4c). Sample MHCS-700 shows higher adsorption capacity and rate than MHCS-600, which is possibly due to the developed graphitic structures that provide electrostatic interaction between π electrons and Cr species.[31]

Based on the data of the Cr(VI) adsorption equilibrium and kinetics of MHCSs listed in Table 3, it can be seen that both the adsorption capacity and rate of sample MHCS-700 are higher than those of MHCS-600 and MHCS-850. On the other hand, after calculating the mass of chromium adsorbed per square meter of adsorbent (based on the specific surface area) after adsorption equilibrium, we found that the values of MHCS-600, MHCS-700 and MHCS-850 are accordingly 0.124, 0.185, 0.184 mg m^{-2}. Interestingly, samples MHCS-700 and MHCS-850 show similar surface utilization degrees, though the former has a surface area twice that of the latter. Clearly, the samples having developed graphitic structures (Fig. 3a) exhibit higher utilization degrees of the surfaces. Therefore, the extraordinary

Table 2 ^{57}Fe Mössbauer parameters of MHCS-700 at room temperature

Oxidation state of iron	IS[a] ($mm\ s^{-1}$)	QS[b] ($mm\ s^{-1}$)	B_{hf} (T)	Spectral area[c] (%)	Component
Fe^0	−0.01	−0.01	33	40	α-Fe
Fe^0	0.18	0.03	21	41	Fe_3C
Fe^{2+}, Fe^{3+}	0.33	−0.02	50	12	Fe_3O_4
Fe^0	−0.11	—	—	7	γ-Fe

[a] IS: isomer shift. [b] QS: electric quadrupole splitting. [c] Uncertainty is ±5% of reported value.

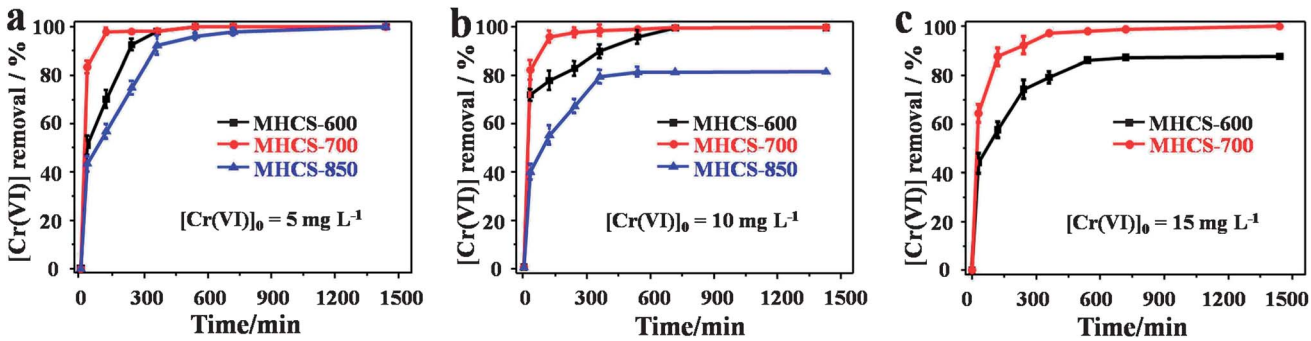

Fig. 4 Relationship between the removal efficiency and time for the adsorption of Cr(VI) by MHCS at initial Cr(VI) concentrations of 5 mg L^{-1} (a), 10 mg L^{-1} (b), 15 mg L^{-1} (c).

adsorption capacity of MHCS-700 may be attributed to two factors: (i) the large specific surface area would provide abundant functional groups, (ii) the developed graphitic structures provide electrostatic interactions between π electrons and Cr species.

Hence, the adsorption isotherms and kinetics of MHCS-700 were studied further in detail. The adsorption kinetics of MHCS-700 could be perfectly fitted by a pseudo-second-order model expressed by eqn (1):

$$\frac{t}{q_t} = \frac{1}{k_2 q_e^2} + \frac{t}{q_e} \tag{1}$$

where, q_e and q_t (mg g^{-1}) are the amounts of Cr(VI) adsorbed on unit mass of the adsorbent when the concentration is equilibrium and at time t (min), respectively; k_2 (g mg^{-1} min^{-1}) is the rate constant of the pseudo-second-order kinetic model.

Fig. 5a show the effectiveness of MHCS-700 in Cr(VI) removal at three initial concentrations (5, 10 and 15 mg L^{-1}) as a function of reaction time at 25 °C. Pictures A–C (inset Fig. 5a) show that the original color of the Cr(VI) solution is yellow. After dispersing MHCS-700 in the Cr(VI) solution, the colour of the solution becomes black. As an external magnet is applied, the black particles are attracted to the side, and the solution becomes colorless. Additionally, it is necessary to note that the MHCS composite nanospheres have good dispersity in Cr(VI) solution (Picture B), which is helpful for the fast adsorption. This directly demonstrates that the MHCSs possessed high adsorption performance and magnetic separability. Fig. 5b shows the plot of adsorption rate as a function of concentration Cr(VI) (5, 10 and 15 mg L^{-1}). It was observed that the adsorption rate of Cr(VI) removal by MHCS-700 was dependent on its initial concentration, and the lower the concentration, the faster the adsorption rate. This could be explained by a mechanism that involved specific metal ion adsorption at a limited number of surface active sites. In other words, with the increase in the Cr(VI) concentration, the high energy sites were firstly saturated and adsorption started on low energy sites, resulting in the decrease in the adsorption rate.[32,33] Meanwhile, the adsorption isotherms of Cr(VI) on MHCS-700 fitted well with the Langmuir model (R^2 > 0.99), as shown in Fig. 5c. This indicated a monolayer adsorption behavior with high adsorption affinity and excellent saturation capacities. The calculated value of Q_m was 200 mg g^{-1}, which was much higher than those of other carbon-based adsorbents reported (Table 4).

The Langmuir model is given by:

$$q_e = \frac{bQ_m C_e}{1 + bC_e} \tag{2}$$

$$\frac{C_e}{q_e} = \frac{1}{Q_m b} + \frac{C_e}{Q_m} \tag{3}$$

where C_e is the equilibrium concentration of Cr(VI) in the supernatant (mg L^{-1}); q_e is the amount of Cr(VI) adsorbed per mass of MHCS-700 composite microspheres (mg g^{-1}) after adsorption equilibrium; Q_m refers to the maximum adsorption capacity corresponding to the quantity of adsorbate required to form a monolayer adsorbed per unit mass of adsorbent (mg g^{-1}).

Table 3 The fitted parameters for equilibrium and kinetic adsorption of Cr(VI) by magnetic hollow carbon nanospheres

Samples	$[Cr(VI)]_0$ (mg L^{-1})	$q_{e,exp}$ (mg g^{-1})	$q_{e,cal}$ (mg g^{-1})	$k_2 \times 10^{-3}$ (g mg^{-1} min^{-1})	R^2	%E (24 h)
MHCS-700	5	27.0	27.1	8.0	0.999	100
	10	51.0	51.1	4.1	0.999	100
	15	76.5	76.7	1.0	0.999	100
MHCS-600	5	26.5	27.4	1.0	0.992	100
	10	50.0	50.2	0.9	0.998	100
	15	61.0	63.0	0.3	0.994	87.8
MHCS-850	5	25.5	26.8	0.7	0.985	100
	10	35.0	41.2	0.5	0.995	81.6

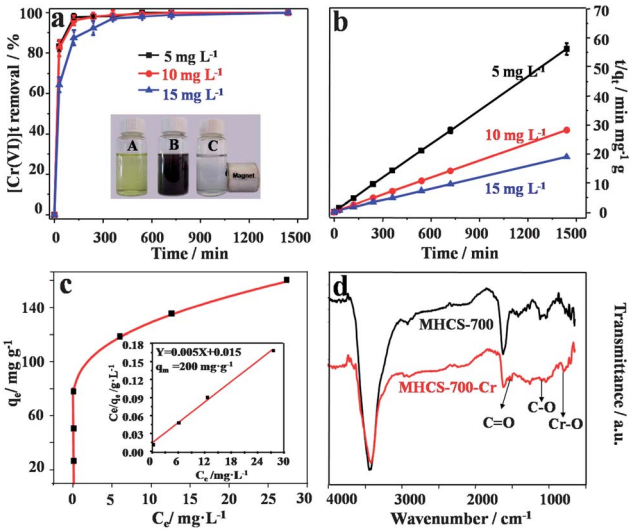

Fig. 5 Effect of initial Cr(VI) concentration (5, 10 and 15 mg L^{-1}) on the Cr(VI) removal efficiency (a), pseudo-second-order linear plot for the removal of Cr(VI) (b), adsorption isotherms at 25 °C (inset: C_e/q_e *versus* C_e plot) for sample MHCS-700 (c), FT-IR spectra of MHCS-700 before and after adsorption of Cr(VI) ions (d).

Table 4 Cr(VI) adsorption capacities of carbonaceous materials from literature

Materials	Cr(VI) (mg g^{-1})	Reference
MHCS-700	200	This work
Activated carbon (AC)	62.97	8
Oxidized AC	15.5	9
Magnetic graphene	0.95	10
γ-Fe_2O_3/CMK-3	30	14
MWCNTs/Fe_2O_3	90	15
Magnetic β-cyclodextrin/graphene oxide	120.19	17

At low pH value (pH = 3), fast protonation of the MHCS surface's active sites X–OH (X = Fe, C) results in the formation of more X–OH_2^+ groups and hence they could adsorb Cr(VI),[34–36] which mainly exists in the form of negatively charged $HCrO_4^-$ ions at low pH (1 < pH < 4).[13,24,37,38] The hollow structure would allow higher exposure efficiency of adsorption site to the adsorbate than a solid one. Hence, the as-obtained MHCSs are capable of rapidly adsorbing Cr(VI) in solution. As the spectrum of MHCS-700 after adsorbing Cr(VI) in Fig. 5d shows, the new absorption at 810 cm^{-1} could be attributed to Cr–O bond vibration, confirming the hypothesis that Cr(VI) ions were adsorbed on the sorbent surface. Meanwhile, the peaks at 1570 and 1120 cm^{-1} are assigned to carboxyl and lactone group vibrations, respectively. There was the possibility that some of the Cr(VI) ions were reduced to Cr(III).[33,39–41] ICP-AES results indicated that there is no detectable chromium, and a total Fe content of 4.8 wt% of MHCS-700 in the solution after the removal of chromium. Hence, the reduced Cr(III) could further conduct ion exchange with the newly formed oxygen functionalities of the carbon surface.[33,42] Such Fe content is about 9 times lower than dissolved Fe from γ-Fe_2O_3/CMK-3 composite[14] under identical adsorption conditions. This demonstrates that our carbon shell builds up a reservoir that effectively restricts the dissolution of Fe into a solution.

4 Conclusions

In this study, highly functionalized hollow polymer spheres could be further engineered to fabricate highly efficient Cr(VI) adsorbents, as demonstrated by MHCSs anchored with magnetic iron-based nanoparticles. Nanosized hollow structures with the merits of high specific surface areas and abundant surface functional groups X–OH (X = Fe, C) can provide more contact and electrostatic adsorption sites for Cr(VI) removal. The iron-based nanoparticles could play a role in the magnetic separation of the MHCSs. When tested as an absorbent for Cr(VI) ion removal, the MHCSs exhibited excellent adsorption capacity. Compared to those samples pyrolyzed at 600 and 850 °C, the MHCS-700 sample showed the highest efficiency for removal of Cr(VI). The extraordinary adsorption capacity of MHCS-700 may be attributed to two factors: (i) the large specific surface area would provide abundant functional groups, (ii) the developed graphitic structures provide electrostatic interactions between π electrons and Cr species. The estimated maximum adsorption capacity Q_m is 200 mg g^{-1}, which is much higher than those of other carbon-based adsorbents in recent literature. Overall, such magnetic hollow carbon spheres with ready magnetism and high surface area can serve as ideal adsorbents for highly efficient removal of Cr(VI).

Acknowledgements

The project was supported by NSFC (no. 21073026), National Natural Science Funds for Distinguished Young Scholar (no. 21225312), and the Program for New Century Excellent Talents in University of China (NCET-09-0254).

Notes and references

1 M. K. Aroua, F. M. Zuki and N. M. Sulaiman, *J. Hazard. Mater.*, 2007, **147**, 752–758.
2 Y. H. Wu, X. H. Ma, M. W. Feng and M. M. Liu, *J. Hazard. Mater.*, 2008, **159**, 380–384.
3 Y. Q. Wang, B. F. Zou, T. Gao, X. P. Wu, S. Y. Lou and S. M. Zhou, *J. Mater. Chem.*, 2012, **22**, 9034–9040.
4 I. Ali, *Chem. Rev.*, 2012, **112**, 5073–5091.
5 Y. X. Lin, W. P. Cai, X. Y. Tian, X. L. Liu, G. Z. Wang and C. H. Liang, *J. Mater. Chem.*, 2011, **21**, 991–997.
6 Y. Zhao, J. R. Peralta-Videa, M. Lopez-Moreno, M. H. Ren, G. Saupe and J. L. Gardea-Torresdey, *Environ. Sci. Technol.*, 2011, **45**, 1082–1087.
7 V. Chandra, J. Park, Y. Chun, J. W. Lee, I. C. Hwang and K. S. Kim, *ACS Nano*, 2010, **4**, 3979–3986.
8 B. V. Babu and S. Gupta, *Adsorption*, 2008, **14**, 85–92.
9 N. Q. Zhao, N. Wei, J. J. Li, Z. J. Qiao, J. Cui and F. He, *Chem. Eng. J.*, 2005, **115**, 133–138.

10 J. H. Zhu, S. Y. Wei, H. B. Gu, S. B. Rapole, Q. Wang, Z. P. Luo, N. Haldolaarachchige, D. P. Young and Z. H. Guo, *Environ. Sci. Technol.*, 2012, **46**, 977–985.
11 J. S. Hu, L. S. Zhong, W. G. Song and L. J. Wan, *Adv. Mater.*, 2008, **20**, 2977–2982.
12 L. F. Chen, H. W. Liang, Y. Lu, C. H. Cui and S. H. Yu, *Langmuir*, 2011, **27**, 8998–9004.
13 C. Y. Cao, J. Qu, W. S. Yan, J. F. Zhu, Z. Y. Wu and W. G. Song, *Langmuir*, 2012, **28**, 4573–4579.
14 M. Baikousi, A. B. Bourlinos, A. Douvalis, T. Bakas, D. F. Anagnostopoulos, J. Tuček, K. Safářŏvá, R. Zboril and M. A. Karakassides, *Langmuir*, 2012, **28**, 3918–3930.
15 V. K. Gupta, S. Agarwal and T. A. Saleh, *Water Res.*, 2011, **45**, 2207–2212.
16 L. Sun, L. Zhang, C. H. Liang, Z. G. Yuan, Y. Zhang, W. Xu, J. X. Zhang and Y. Z. Chen, *J. Mater. Chem.*, 2011, **21**, 5877–5880.
17 L. L. Fan, C. N. Luo, M. Sun and H. M. Qiu, *J. Mater. Chem.*, 2012, **22**, 24577–24583.
18 G. H. Wang, Q. Sun, R. Zhang, W. C. Li, X. Q. Zhang and A. H. Lu, *Chem. Mater.*, 2011, **23**, 4537–4542.
19 R. Liu, S. M. Mahurin, C. Li, R. R. Unocic, J. C. Idrobo, H. J. Gao, S. J. Pennycook and S. Dai, *Angew. Chem., Int. Ed.*, 2011, **50**, 6799–6802.
20 N. Jayaprakash, J. Shen, S. S. Moganty, A. Corona and L. A. Archer, *Angew. Chem., Int. Ed.*, 2011, **50**, 5904–5908.
21 A. H. Lu, W. Li, A. Kiefer, W. Schmidt, E. Bill, G. Fink and F. Schüth, *J. Am. Chem. Soc.*, 2004, **126**, 8616–8617.
22 A. H. Lu, W. Schmidt, N. Matoussevitch, H. Bönnermann, B. Spliethoff, B. Tesche, E. Bill, W. Kiefer and F. Schüth, *Angew. Chem., Int. Ed.*, 2004, **43**, 4303–4306.
23 J. Cao and W. X. Zhang, *J. Hazard. Mater.*, 2006, **132**, 213–219.
24 S. Fiorilli, B. Onida, B. Bonelli and E. Garrone, *J. Phys. Chem. B*, 2005, **109**, 16725–16729.
25 Q. Sun, G. H. Wang, W. C. Li, X. Q. Zhang and A. H. Lu, *J. Nat. Gas Chem.*, 2012, **21**, 251–256.
26 A. H. Lu, W. C. Li, G. P. Hao, B. Spliethoff, H. J. Bongard, B. B. Schaack and F. Schüth, *Angew. Chem., Int. Ed.*, 2010, **49**, 1615–1618.
27 K. Kadirvelu and C. Namasivayam, *Adv. Environ. Res.*, 2003, **7**, 471–478.
28 A. H. Lu, W. Li, N. Matoussevitch, B. Spliethoff, H. Bönnemann and F. Schüth, *Chem. Commun.*, 2005, 98–100.
29 A. H. Lu, W. Li, E.-L. Salabas, B. Spliethoff and F. Schüth, *Chem. Mater.*, 2006, **18**, 2086–2094.
30 J. Kim, H. S. Kim, N. Lee, T. Kim, H. Kim, T. Yu, I. C. Song, W. K. Moon and T. Hyeon, *Angew. Chem., Int. Ed.*, 2008, **47**, 8438–8441.
31 H. L. Ma, Y. W. Zhang, Q. H. Hu, D. Yan, Z. Z. Yu and M. L. Zhai, *J. Mater. Chem.*, 2012, **22**, 5914–5916.
32 I. A. Zouboulis, K. N. Lazaridis and K. A. Matis, *J. Chem. Technol. Biotechnol.*, 2002, **77**, 958–964.
33 Y. B. Liu, Y. Q. Wang, S. M. Zhou, S. Y. Lou, L. Yuan, T. Gao, X. P. Wu, X. J. Shi and K. Wang, *ACS Appl. Mater. Interfaces*, 2012, **4**, 4913–4920.
34 W. F. Liu, J. Zhang, C. L. Zhang and L. Ren, *Chem. Eng. J.*, 2012, **189–190**, 295–302.
35 H. L. Ma, Y. W. Zhang, Q. H. Hu, D. Yan, Z. Z. Yu and M. L. Zhai, *J. Mater. Chem.*, 2012, **22**, 5914–5916.
36 K. V. Kumar, *J. Hazard. Mater.*, 2006, **137**, 1538–1544.
37 Y. S. Ho, *J. Hazard. Mater.*, 2006, **136**, 681–689.
38 R. L. Ramos, J. Martinez and R. M. G. Coronado, *Water Sci. Technol.*, 1994, **30**, 191–197.
39 D. Park, S. R. Lim, Y. S. Yun and J. M. Park, *Bioresour. Technol.*, 2008, **99**, 8810–8818.
40 L. Zhang, N. Wu and H. Wei, *Environ. Sci. Technol.*, 2012, **46**, 419–425.
41 R. Liu, S. M. Mahurin, C. Li, R. R. Unocic, J. C. Idrobo, H. J. Gao, S. J. Pennycook and S. Dai, *Angew. Chem., Int. Ed.*, 2011, **50**, 6799–6802.
42 N. H. Hsu, S. L. Wang, Y. C. Lin, G. D. Sheng and J. F. Lee, *Environ. Sci. Technol.*, 2009, **43**, 8801–8806.